Applied Catalysis B: Environmental 125 (2012) 311–323

Contents lists available at SciVerse ScienceDirect

Applied Catalysis B: Environmental

journal homepage: www.elsevier.com/locate/apcatb

Isomorphous substitution of Zr in the framework of aluminosilicate HY by an electrochemical method: Evaluation by methylene blue decolorization

N. Sapawe[a], A.A. Jalil[a,*], S. Triwahyono[b], S.H. Adam[a], N.F. Jaafar[b], M.A.H. Satar[a]

[a] Institute of Hydrogen Economy, Faculty of Chemical Engineering, Universiti Teknologi Malaysia, 81310 UTM Johor Bahru, Johor, Malaysia
[b] Ibnu Sina Institute for Fundamental Science Studies, Faculty of Science,Universiti Teknologi Malaysia, 81310 UTM Johor Bahru, Johor, Malaysia

ARTICLE INFO

Article history:
Received 5 March 2012
Received in revised form 20 May 2012
Accepted 27 May 2012
Available online 15 June 2012

Keywords:
Isomorphous substitution
$EGZrO_2$/HY
Electrochemical
Photodecolorization
Methylene blue

ABSTRACT

Isomorphous substitution of Zr in the framework of aluminosilicate HY occurred during the preparation of electrogenerated zirconia supported HY ($EGZrO_2$/HY) catalyst via a simple electrochemical method. Dealumination accompanied by an ion exchange with Zr^{4+} formed Si—O—Zr bond, which controlled the formation of active species $EGZrO_2$ that influenced the efficiency of the photodecolorization of methylene blue (MB). An amount of 0.375 g L^{-1} 1 wt% $EGZrO_2$/HY was found to be the optimum dosage for 10 mg L^{-1} MB, which resulted in 97% decolorization after 6 h of contact time at pH 11. The kinetics study indicates that the reaction follows the Langmuir–Hinshelwood model, where the reaction may occur both on the surface of the catalyst and in the bulk solution. The mineralization of MB was measured by removal of chemical oxygen demand (COD), five days biochemical oxygen demand/chemical oxygen demand (BOD_5/COD), and total organic carbon (TOC/TOC_0), and the results obtained were 95%, 7.14, and 0.08, respectively. After five cycling runs, the catalyst was still stable and showed no leaching effect. This study is believed to be extendable to the synthesis of other catalysts with different characteristics and be used in various applications.

1. Introduction

Over the past few decades, environmental issues involving water pollution have become an important issue. The major pollutants in wastewater, such as organic dyes, are produced from the dyeing processes in which approximately 15% of the total world production of dyes is released in textile effluents [1,2]. Approximately 97% of local dye effluents are produced by the food, chemical, and textile industries [3]. Among these industries, approximately 22% of the total volume of wastewater is produced by the textile industry, which commonly uses basic dyes such as crystal violet, rhodamine B, methyl violet, and methylene blue, to dye wool, silk, cotton, linen, and modified acrylic fibers [4]. Most of the unused dye results in undesirable effluents and is discharged into the environment with or without further treatment. These effluents run into natural water bodies and can cause severe problems if not treated properly because the dyes are toxic, mutagenic and carcinogenic to human life [5] as well as prohibit the photosynthesis of aquatic life when present even in small quantities like 1 ppm [6]. To overcome this problem, several methods for the removal of dyes have been reported, including chemical and biological oxidation [7], adsorption [8], coagulation and flocculation [9], electrochemical oxidation [10], ion exchange [11], and membrane separation [12]. However, these methods have their own limitations including being time-consuming, expensive, and commercially unattractive as well as resulting in the generation of secondary wastes.

Advanced oxidation processes (AOPs) using semiconductors such as TiO_2, ZnO, WO_3, Fe_2O_3, CuO, ZrO_2, CdS, In_2O_3, and SnO_2 as photocatalysts have become important because the AOPs can convert a wide range of harmful dyes into non-toxic products, CO_2 and water at ambient temperature [13–15]. Mixed metal oxides such as TiO_2–ZrO_2, Ag–ZnO, Fe_2O_3–TiO_2, TiO_2–ZnS, Sn–ZnO, and Ag–TiO_2 exhibit better performance and enhance photocatalytic activity [16–21]. The use of mesoporous materials such as zeolite as a support for the metal oxides has recently become the focus of intensive research because the catalyst support influences the catalytic performance through structural features and the interaction between the materials leads to the enhancement of the contact between the surface and irradiation [22] as well as reduction in the amount of metal oxides required [15]. Zeolitic supports are important because of their high surface area, thermal stability, eco-friendly nature, specific photophysical properties, and their potential ability to control charge and electron transfer processes [23,24]. A review of recent studies has revealed that some of the

* Corresponding author. Tel.: +60 7 5535581; fax: +60 7 5536165.
E-mail address: aishah@cheme.utm.my (A.A. Jalil).

0926-3373/$ – see front matter © 2012 Elsevier B.V. All rights reserved.
http://dx.doi.org/10.1016/j.apcatb.2012.05.042

important metal oxide-supported zeolites include TiO_2-HZSM-5, Co-ZSM-5, CuO-X zeolite, and Fe-exchange zeolite [21,25–27]. The popular metal oxides use TiO_2 and ZnO but alternative photocatalysts are still under development and more research is required. ZrO_2 exhibits great potential because of specific optical and electrical properties, thermal stability, and strong mechanical strength as well as the presence of acid–base and redox capabilities [28,29]. To the best of our knowledge, reports on ZrO_2-supported zeolite photocatalysts are still scarce.

Recently, there has been increasing interest in the use of ZrO_2 nanosized photocatalyst in photocatalytic activity because of some principal factors such as increase in surface area and quantum effect, thus enhancing their photoreactivity properties [30,31]. There are various methods of synthesizing nanosized zirconia particles, such as sol–gel, co-precipitation, ball milling, hydrothermal process, gas phase synthesis, microemulsion methods, and emulsion-assisted direct precipitation [28] that have been reported, but there are still very few studies on the preparation of nanosized zirconia particle using an electrochemical method.

We have reported a new method for preparing very fine particles of zinc metal with high reactivity using a simple electrochemical method, and the successful use of a catalyst to synthesize anti-inflammatory agents via cross-coupling reactions [32]. In addition, we found that the zinc oxide nanoparticles prepared by the same method led to the generation of protonic acid sites on HZSM-5 supports resulting in enhancement of *n*-alkane isomerization [33]. Recently, we also found that α-Fe_2O_3 supported HY catalyst exhibits high photoactivity towards the decolorization of methyl orange [34]. The nanosized particles of those metals might play an important role in the reactions. These findings have led to an interest in exploring the synthesis of other nanometal oxides supported on zeolites for photocatalytic reactions. Therefore, the present study reports for the first time, the preparation of a nanoparticle electrogenerated ZrO_2-supported HY zeolite ($EGZrO_2$/HY) catalyst using the corresponding method. The prepared catalyst was characterized by X-ray diffraction (XRD), transmission electron microscopy (TEM), Fourier transform infrared (FT-IR), ultraviolet–visible diffuse reflectance spectroscopy (UV–vis/DRS), Brunnauer–Emmett–Teller surface area analysis (BET), ^{29}Si and ^{27}Al magic angle spinning nuclear magnetic resonance (MAS NMR), X-ray photoelectron spectroscopy (XPS), and inductively coupled plasma mass spectrometry (ICP-MS). The activity of the catalyst for the photodecolorization of methylene blue (MB) was studied under various conditions to determine the effect of pH, metal loading, catalyst dosage, and initial dye concentration. The kinetics behavior of the catalyst was also studied to determine the surface interaction of the catalyst with MB. Herein, we report the advantage of using the electrochemical preparation method and the effect of the support material on the structure of the $EGZrO_2$/HY catalyst. A new structural model for $EGZrO_2$/HY is proposed that is consistent with the results from characterization of the catalyst and takes into account dealumination and ion exchange.

2. Experimental

2.1. Materials

The HY zeolite had a Si/Al ratio of 80 and was purchased from Zeolyst International. *N*,*N*-dimethylformamide (DMF) was purchased from Merck Sdn. Bhd. Malaysia, and naphthalene was obtained from Fluka Sdn. Bhd., Malaysia. Sodium hydroxide (NaOH), hydrochloric acid (HCl), and methylene blue (C.I. 52015 for microscopy) were obtained from QReC™. The platinum (Pt) and zirconia (Zr) plate cells were obtained from Nilaco Metal, Japan. Degussa P25 TiO_2 was obtained from Acros Organics, Belgium. All reagents were of analytical grade and were used as received. Deionized water was used for the preparation of the pH solution and adjustments to the pH were performed using a 0.1 M HCl and NaOH solution.

Table 1
Time required for complete electrolysis and the exact amount of $EGZrO_2$ loading onto HY as detected by ICP-MS.

$EGZrO_2$ (wt %)	Time for complete electrolysis[a] (min)	% Zr detected in catalyst[b]
1	2.23	1.02
8	19.2	7.98
15	38.9	15.3
22	62.0	22.0

[a] Calculated based on Faraday's law (Eq. (1)).
[b] Zr detected determine by ICP-MS.

2.2. Catalyst preparation

$EGZrO_2$ was prepared following a previously reported protocol [30]. A DMF solution (10 mL) containing 0.1 M tetraethylammonium perchlorate was electrolyzed in the presence of a naphthalene mediator (6 mmol) in a normal one-compartment cell fitted with a Pt plate cathode (2 cm × 2 cm) and Zr plate anode (2 cm × 2 cm) at a constant current density of 120 mA/cm^2 under a nitrogen atmosphere at 273 K. After electrolysis, the mixture was impregnated, oven dried overnight at 378 K, and calcined at 823 K for 3 h to yield a white powder ($EGZrO_2$) for characterization and photocatalytic testing.

The $EGZrO_2$/HY catalyst was prepared using the same procedure except for the addition of the HY zeolite (1.5 g) prior to electrolysis, and a white powder was obtained as the final product. The required weight percent of the $EGZrO_2$ supported on HY and the time required for complete electrolysis was calculated based on Faraday's law of electrolysis (Table 1),

$$t = \left(\frac{F}{I}\right)(z \times n) \quad (1)$$

where t = total time for the constant current applied (s); F = 96,486 C mol^{-1}, which is the Faraday constant; I = the electric current applied; z = the valency number of ions of substances (electrons transferred per ion); and n = the amount of substance (no of moles, liberated $n = m/M$).

2.3. Characterization

The crystalline structures of the catalysts were studied by XRD recorded on a D8 ADVANCE Bruker X-ray diffractometer using Cu Kα radiation at a 2θ angle ranging from 3° to 90°. The particle sizes of the catalysts were calculated using the Debye–Scherrer equation,

$$D = \frac{k\lambda}{\beta \cos\theta} \quad (2)$$

where k = 0.94 is a coefficient, λ = 1.5406 Å is the X-ray wavelength, β is the full width half maximum (FWHM) of the sample and θ is the diffracting angle. The phases were identified with the aid of the Joint Committee on Powder Diffraction Standards (JCPDS) files.

The morphological properties of nanosized $EGZrO_2$ and the $EGZrO_2$/HY catalyst as well as the distribution of $EGZrO_2$ deposited on the HY surface were examined by TEM (JEOL JEM-2100F). FT-IR (PerkinElmer Spectrum GX FTIR Spectrometer) was performed using the KBr method with a scan range of 400–4000 cm^{-1}. The optical absorption properties of the catalyst were obtained

using UV–vis/DRS (PerkinElmer Spectrophotometer) in the range of 200–800 nm at room temperature. The band gap of $EGZrO_2$ was determined from plots of the Kubelka–Munk (K–M) function [$f_{K-M} = (h\nu/\lambda)^{1/2}$] as a function of the energy of the excitation light [$h\nu$].

The textural properties (i.e., specific surface area, external surface area, micropore area, micropore volume, pore volume, and pore diameter) were determined from nitrogen adsorption–desorption isotherms at liquid nitrogen temperature using a Micromeritics ASAP 2010 instrument. The surface area was calculated with the BET method, and pore distributions were determined by the Barrett–Joyner–Halender (BJH) method whereas the micropore area, micropore volume, and external surface area were estimated by *t*-plots. Prior to measurement, all the samples were degassed at 110 °C to 0.1 Pa. ^{29}Si and ^{27}Al MAS NMR spectra were recorded on a Bruker Solid NMR (JEOL 400 MHz) spectrometer using tetramethylsilane (TMS) as an external reference at room temperature. The chemical oxidation state of the $EGZrO_2$/HY catalyst was determined using XPS conducted on a Kratos Ultra spectrometer equipped with a Mg Kα radiation source (10 mA, 15 kV) in the range of 0–800 eV. The powdered sample was pressed into a small Inox cylinder and analyzed inside an analysis chamber at 1×10^{-10} Pa during data acquisition. To correct the energy shift due to surface charging of the samples, the binding energy of the C1s peak at 284.5 ± 0.1 eV was taken as the internal standard.

2.4. Photocatalytic testing

The photocatalytic activity of the prepared $EGZrO_2$/HY catalyst was tested for the decolorization of MB. A 0.075-g sample of the catalyst was dispersed in 200 mL of 10 mg L^{-1} MB aqueous solution. The adsorption–desorption equilibrium was achieved under dark conditions after 2 h, and the mixture was irradiated at room temperature for 6 h with constant stirring using a 500-W high pressure Hg lamp UV light coupled with a cooler system (USH-500SC Mercury Lamp 8.5 A with emission at 350–400 nm). The distance between the light and the reaction vessel was 15 cm. At specific time intervals, 2.5 mL of the sample solution was withdrawn and centrifuged prior measurements of the MB concentration by a UV–vis spectrophotometer (Thermo Scientific Genesys 10 UV Scanning) using the characteristic adsorption band at 664 nm. The decolorization percentage was calculated as follows,

$$\text{Decolorization}(\%) = \frac{(C_0 - C_t)}{C_0} \times 100 \quad (3)$$

where C_0 represents the initial concentration and C_t denotes a variable concentration.

2.5. Analyses

The elemental analyses of Zr in a catalyst and a solution during an experiment were determined by ICP-MS using ELAN 6100 PerkinElmer ICPMS. The BOD of the solution were measured using YSI model 33, whereas the BOD bottles were incubated at 20 °C for five days and the difference in dissolved oxygen was used to calculate BOD_5. The HACH DR4000 spectrometer was used for COD measurement. In addition, the total organic carbon (TOC) removal was determined using a TOC Shimadzu Vcph spectrophotometer for each run before and after a 6 h reaction time for the evaluation of the mineralization of MB dye. TOC was calculated as the difference between the total carbon (TC) and inorganic (IC) in the liquid sample.

Table 2
The crystallite size and d_{101} value of the catalysts.

Catalysts	Crystallite size (nm)	d_{101} value (Å)
$EGZrO_2$	12.3	2.95
HY Zeolite	33.2	–
1 wt% $EGZrO_2$/HY	17.2	2.96
8 wt% $EGZrO_2$/HY	10.7	2.96
15 wt% $EGZrO_2$/HY	10.7	2.96
22 wt% $EGZrO_2$/HY	9.55	2.95

3. Results and discussion

3.1. Characterization

3.1.1. Crystallinity, phase, and structural studies

The XRD pattern of the prepared $EGZrO_2$/HY catalyst was compared with $EGZrO_2$ and bare HY, and the results are shown in Fig. 1. The peak intensity of HY decreased as the $EGZrO_2$ loading increased because the presence of foreign substances affected the morphology of the supported HY fingerprint (Fig. 1a). A series of characteristic peaks were observed for $EGZrO_2$ at 30.2° (1 0 1), 35.2° (1 1 0), 50.3° (1 1 2), and 60.2° (2 1 1), which are consistent with the tetragonal phase of ZrO_2 (JCPDS 36-1541) (Fig. 1b and c). Characteristic peaks were observed at 2θ equal to 28.2°, 31.5°, and 34.5° and corresponded to the diffraction patterns of (−1 1 1), (1 1 1), and (0 0 2) of the monoclinic phase of ZrO_2 (Fig. 1b) [35]. No other diffraction peaks were detected, which indicated the purity of the prepared $EGZrO_2$.

It is reported that Si plays an important role in the formation of the tetragonal phase while inhibiting the formation of the monoclinic phase [36]. The interaction between $EGZrO_2$ with Si framework may cause the elimination of the unstable monoclinic phase but did not affect the tetragonal phase of $EGZrO_2$ (Fig. 1b and c). The average crystallite size of the catalysts was estimated by the Debye–Scherrer equation on the basis of the major peak of *t*-ZrO_2 (1 0 1) at 2θ = 28.2 to have d_{101} values of approximately 2.96 Å, and these values are listed in Table 2. The crystallite size decreased as the $EGZrO_2$ loading increased, and the values range from 17.2 to 9.55 nm because of the interaction between the zirconia species and HY [37].

3.1.2. Morphological properties

The morphological properties of $EGZrO_2$ and the $EGZrO_2$/HY catalyst were examined by high resolution-transmission electron microscopy (HR-TEM), and the images are presented in Fig. 2. Fig. 2a illustrates that $EGZrO_2$ was successfully prepared with well-defined boundaries and no connecting necks, which indicated the absence of the sintering effect between the particles. The average particle size for $EGZrO_2$ varied in a narrow range from 8 to 18 nm. The theoretical value of the particle size (D) was found to be 19.2 nm, which was estimated by the following equation,

$$D = \frac{6}{\rho S} \quad (4)$$

where ρ the theoretical density of the $EGZrO_2$ powder and S is the surface area determined by N_2 adsorption–desorption isotherms, assuming that the particles are spherical in shape [38].

However, the micrographs show particles with an elliptical and irregular shape, which may be due to the particles overlapping [28]. The value of the interplanar distance (d-spacing) of the lattice fringes estimated from this image was consistent with the value of lattice spacing of tetragonal and monoclinic $EGZrO_2$ obtained from the XRD analysis (Fig. 2b and Table 3). However, a minor difference in the crystallite size obtained from XRD and HRTEM measurements were observed, which may be due to the presence of agglomeration in the prepared sample [28].

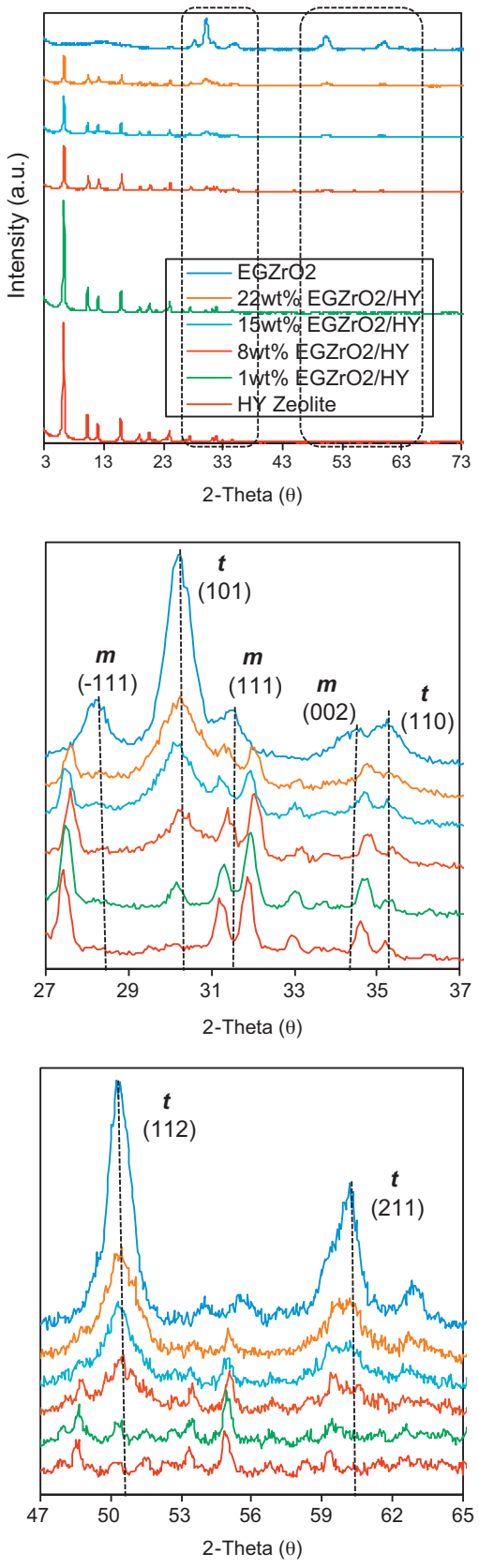

Fig. 1. XRD patterns of catalysts: (a) full range 3–73° (b) range 27–37° (c) range 47–65°.

Table 3
The d-value of $EGZrO_2$ lattice obtained from XRD and HR-TEM analysis.

Phase of $EGZrO_2$	2-Theta (θ)[a]	d_{hkl}[a] (Å)	d-spacing[b] (nm)
m (−1 1 1)	28.2	3.16	0.320
t (1 0 1)	30.2	2.95	0.296
m (1 1 1)	31.3	2.83	0.276
m (0 0 2)	34.5	2.59	0.255
t (1 1 0)	35.2	2.54	0.256
t (1 1 2)	50.3	1.81	0.190
t (2 1 1)	60.2	1.54	0.146

[a] Value obtained from XRD analysis.
[b] Lattice fringes obtained from HR-TEM analysis.

The inset figures correspond to the fast Fourier transform patterns (FFT) and indicated that the materials have either a crystalline (Fig. 2a, e, and g) or an amorphous (Fig. 2c) phase. Magnification of the selected area in the FFT showed the atomic arrangement in the crystal and allowed for estimation of the interplanar distance (Fig. 2b, f, and h). The value of the lattice fringes was consistent with the d-spacing for $EGZrO_2$, which is tabulated in Table 3. This agreement confirms that the $EGZrO_2$ nanoparticles were well dispersed on the HY support (Fig. 2e and g).

3.1.3. Vibrational spectroscopy

FT-IR spectroscopy is a very useful technique for obtaining vibrational information about the species in materials. Therefore, the prepared catalysts were subjected to FT-IR analysis, and the results are shown in Fig. 3. For $EGZrO_2$, a weak peak was observed at 1028 cm^{-1}, which may correspond to the Zr=O stretching vibration. The peaks observed in the range of 450–520 cm^{-1} may correspond to the Zr—O bond (Fig. 3b) [28,39]. The peaks corresponding to the tetragonal phase (*t*-ZrO_2) were observed at 580 and 520 cm^{-1}, and the peak corresponding to the monoclinic phase (*m*-ZrO_2) was observed at 747 cm^{-1} [39]. These results support the XRD analysis data, which is indicative of the purity of the $EGZrO_2$ sample.

The $EGZrO_2$/HY catalyst showed a broad band at 3445 cm^{-1} because of the H_2O molecules adsorbed on catalyst surface and 1634 cm^{-1} which attributed to vibrational distortion of the O—H groups on the catalyst surface (Fig. 3a). The weak bands between 800 and 400 cm^{-1}, which correspond to the Si—O—Si flexural vibration, decreased in intensity as the $EGZrO_2$ loading increased because of the superposition of Zr—O and Si—O bonds (Fig. 3b) [40]. A significant decrease in the intensity of the peak at 1079 cm^{-1} was observed after $EGZrO_2$ loading, which suggested a possible interrelationship of $EGZrO_2$ on the Si—O—Si group (Fig. 3b) [40]. This result suggests that Zr may be inserted into the zeolite framework during electrolysis [41]. However, no obvious band was observed in the region of 965, 1015 and 1025 cm^{-1}, which correspond to the vibration of the Si—O—Zr bond. It may be because of overlapping with zeolitic material characteristic stretching frequencies in this region [42]. For further investigation, the samples were evacuated at 673 K for 1 h prior to IR measurement to remove the physisorbed water, and the results are shown in Fig. 3c. The sharp peak at 3745 cm^{-1} was shifted to a lower wavenumber (3740 cm^{-1}) and the intensity increased with increasing $EGZrO_2$ loading, which could be attributed to a weak interaction between the isolated silanol groups located at the surface and the neighboring metal species (Zr) [43]. According to Krijnen, the shift in this peak to 3740 cm^{-1} may also suggest that dealumination has occurred in the zeolite [44]. The peak at 3700 cm^{-1} decreased in intensity as the metal loading increased, which may correspond to the interaction of Zr species with weak hydrogen bridges in defect sites of hydroxyl groups. A new peak appeared at 3685 cm^{-1}, which increased in intensity with increasing $EGZrO_2$ loading, indicating the increase of the hydroxyl groups of the extra framework aluminum species

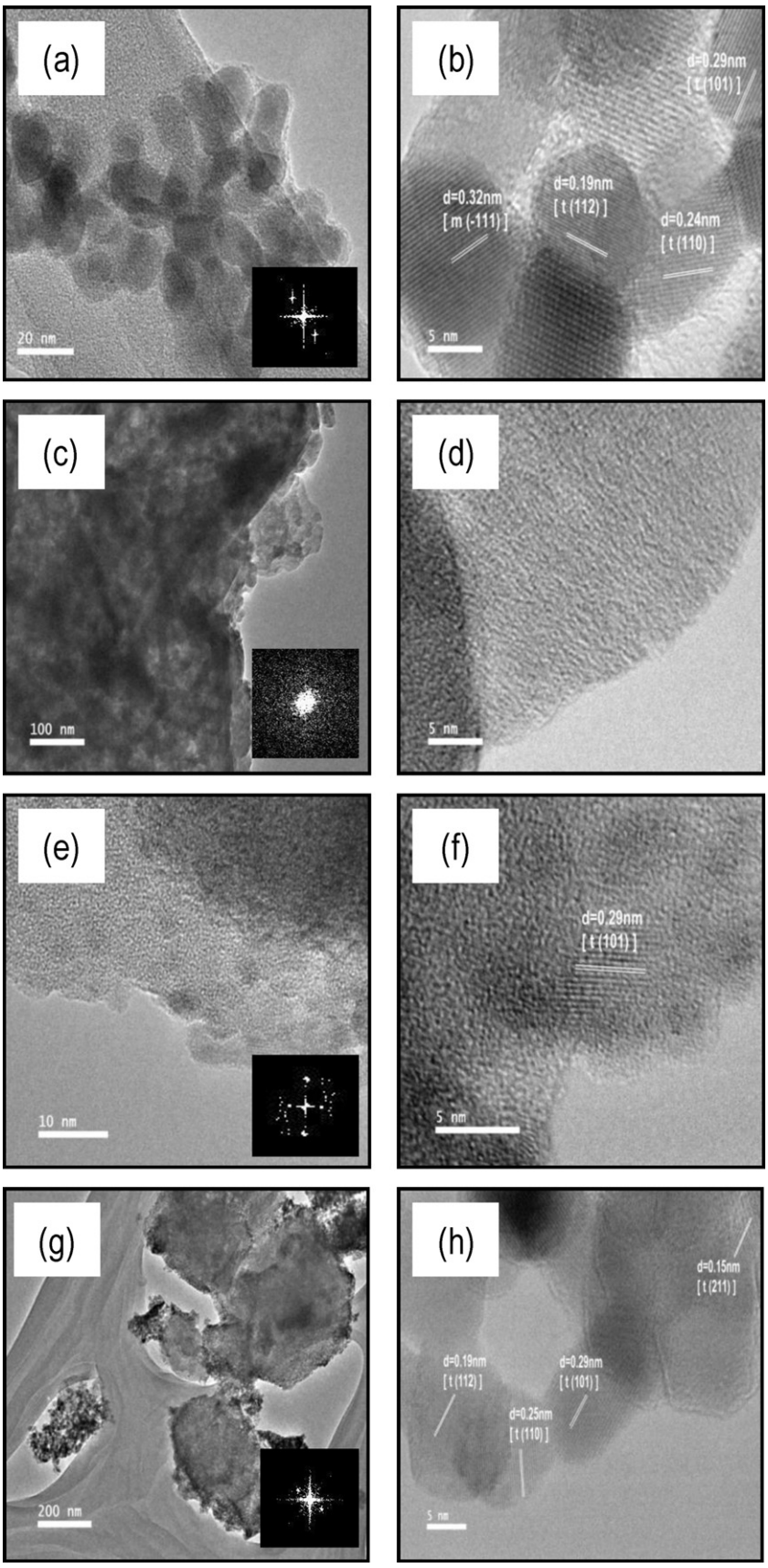

Fig. 2. HR-TEM micrographs of catalysts in low and high magnification for (a and b) $EGZrO_2$, (c and d) HY zeolite, and (e–h) $EGZrO_2$/HY. The inset of (a, c, e, and g) are its corresponding FFT.

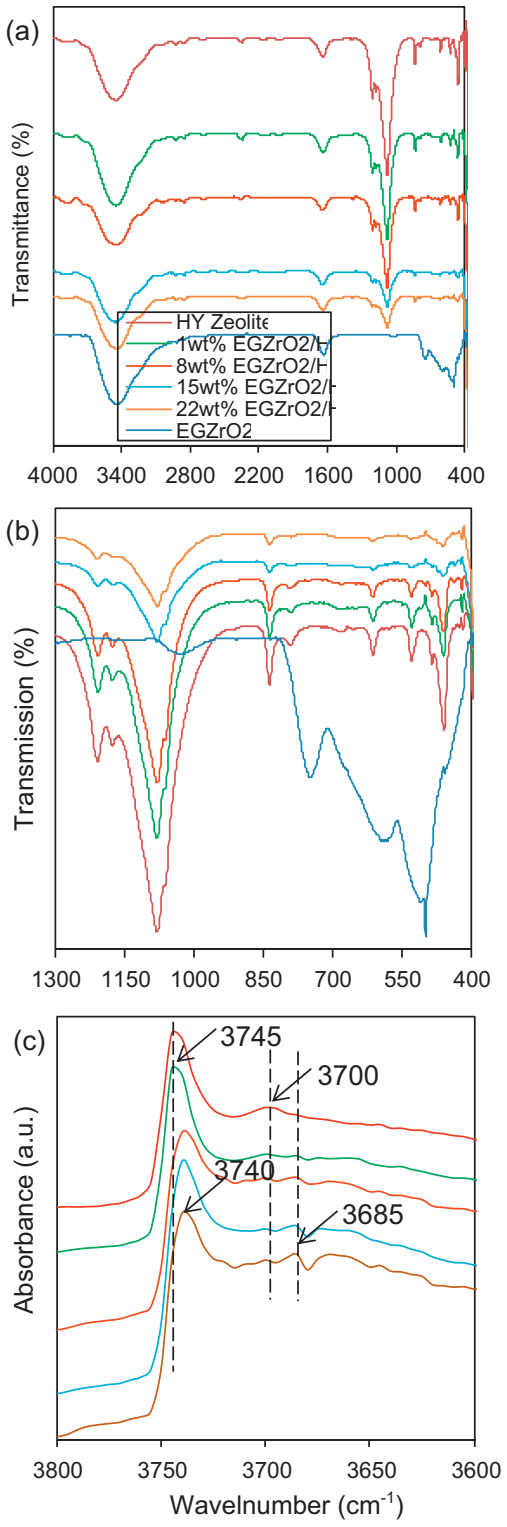

Fig. 3. FT-IR spectra of catalysts at region (a) 4000–400 (b) 1300–400, and (c) 3800–3600 nm (evacuated system).

(Al(O)OH) caused by the isomorphous substitution between Zr and Al ions in the framework [44].

3.1.4. Nuclear magnetic resonance

To elucidate the structure of the prepared catalyst, ^{29}Si and ^{27}Al MAS NMR spectra were obtained for the 22 wt% $EGZrO_2$/HY with respect to bare HY. ^{29}Si MAS NMR chemical shifts were used to define the Si environments and provide information regarding the coordination of Si with other Si atoms or Al atoms. As illustrated in Fig. 4a, the intensity of the sharp peak observed for bare HY at −107 ppm was reduced by approximately one-third upon introduction of $EGZrO_2$, which could indicate a chemical interaction reducing the total amount of Si(0Al) groups [45]. The trace peaks at −101 and −95 ppm, which correspond to the Si(1Al) and Si(2Al) groups, also disappeared (Fig. 4a). This result is in agreement with the FT-IR analysis in which the intensity of the peak observed between 800 and 400 cm^{-1} corresponding to the Si—O—Si bond decreased as the $EGZrO_2$ loading increased. ^{27}Al MAS NMR was employed to distinguish the Al in framework sites (tetrahedral) from extra framework sites (octahedral). In Fig. 4b, the peak corresponding to the tetrahedral Al framework in HY was partially eliminated when $EGZrO_2$ was added. However, no other peaks were detected signifying neither the presence of octahedral extra framework aluminum nor reinsertion of the eliminated aluminum into the Si framework [46,47]. As reported by Klinowski, the eliminated aluminum may be present as invisible aluminum in the form of $Al(OH)_3$, $Al(OH)^{2+}$, $Al(OH)^{+}_2$, and Al_2O_3 or some polymeric aluminous species [45].

In order to clarify the isomorphous substitution between Zr and Al, the amount of unbounded Zr and Al in the HY framework was studied using 22 wt% $EGZrO_2$/HY catalyst. The corresponding catalyst was stirred in DMF solution for approximately 30 min and then filtered before subjected to ICP-MS analysis. It was found that approximately 1.66×10^{20} Zr atoms were detected in the filtrate solution, referring to the unbounded $EGZrO_2$ (5.9%). Therefore, 94.1% of total Zr ions in 22 wt% $EGZrO_2$/HY catalyst were exchanged with the Al in the HY framework. However, the number of Al atoms detected from the same solution was only 2.18×10^{21}, which is less than expected numbers of Al that were exchanged with the Zr in the aluminosilicate framework. The loss (17%) of Al is most probably due to the formation of polymeric aluminous compounds that could not pass through the filter as reported in NMR studies. All the calculations were based on the ratio of element in the HY $(Al_7Si_{17}O_{48})\cdot 32(H_2O)$.

3.1.5. Chemical oxidation state determination

The dealumination of the zeolite after the addition of zirconia was confirmed by the FT-IR and NMR data. XPS analysis was performed to determine the chemical states of the surface Zr in the catalyst. Fig. 5 shows the XPS spectra of Zr 3d and O1s for the 22 wt% $EGZrO_2$/HY catalyst. A doublet peak with binding energies of 182.8 eV (Zr $3d_{5/2}$) and 184.9 eV (Zr $3d_{3/2}$) was observed, which exactly matches the chemical oxidation state of Zr^{4+} ions [48]. However, the observed value for the $EGZrO_2$/HY sample was slightly shifted to higher binding energies by 0.6 eV compared to pure zirconium oxide (182.2 eV), which suggests an interaction between the $EGZrO_2$ and HY [29,49]. Because Si is more electronegative than zirconium, a Si—O— bond in a Zr environment is expected to withdraw more electron density than in a Zr—O environment, which is the case for pure ZrO_2, and implies a shift of the Zr $3d_{5/2}$ binding energies to higher values [50]. In addition, the spectra of O1s were obtained to differentiate the bonded oxygen atoms in silica environments. The photoelectron spectra of O1s shown in Fig. 5 displays two peaks that correspond to Si—O—Zr and Si—O—Si with binding energies of 529.8 and 532.3 eV, respectively [51,52]. Therefore, it was confirmed that the Si—O—Zr groups were present in the catalyst material.

3.1.6. Proposed structure of $EGZrO_2$/HY

Analogous to our previous study [32], probable reaction pathways of the preparing $EGZrO_2$ are shown in Fig. 6. Electrolysis of a DMF solution with a Pt cathode and a Zr anode results in anodic dissolution of Zr metal to give Zr ions. On the other hand,

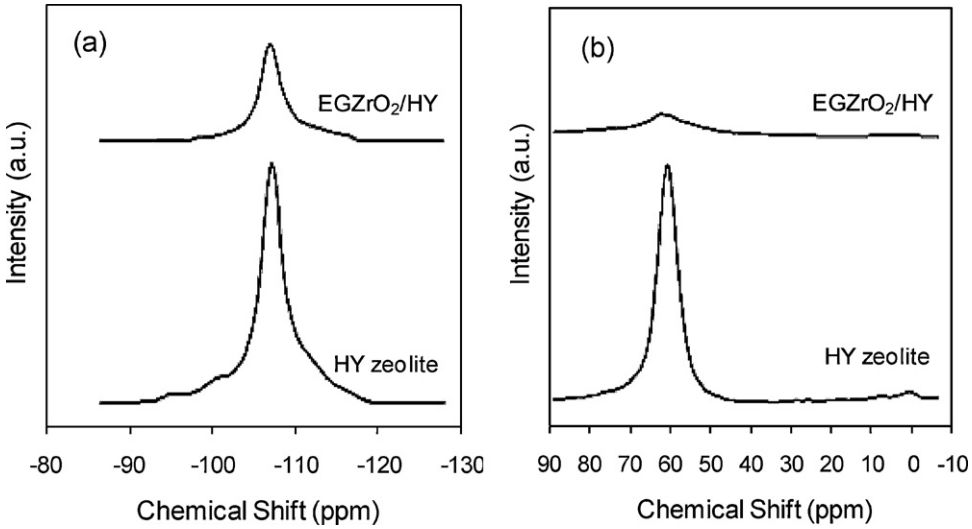

Fig. 4. MAS NMR spectra of (a) ^{29}Si and (b) ^{27}Al of bare HY and 22 wt% $EGZrO_2$/HY catalyst.

at the cathode, a one-electron reduction of naphthalene molecule occurs to give radical anion of naphthalene, which was shown by the appearance of a dark green color on the surface of the cathode. Reduction of Zr ion with naphthalene radical anion gives zero-valent reactive $EGZrO_2$. In parallel, a part of the Zr^{4+} ions takes part in the isomorphous substitution to form $EGZrO_2$/HY catalyst.

The proposed structure of the $EGZrO_2$/HY catalyst is based on the analyses data mentioned above. The FT-IR results obtained were in agreement with the data reported by Krijnen in which the shifted peak from 3745 cm^{-1} to 3740 cm^{-1} signifies the occurrence of dealumination in the zeolite framework, and the appearance of a new peak at 3685 cm^{-1} indicates the presence of extra framework aluminum species [44]. In addition, the XPS spectra of Zr 3d and O1s established the chemical oxidation state of the Zr^{4+} ions and the presence of the Si—O—Zr group, respectively. Therefore, it was proposed that Al was extracted from the HY framework creating vacant sites that are then filled by Zr^{4+} during the electrolysis (Fig. 6). The partial dealumination designated by ^{29}Si and ^{27}Al MAS NMR spectra and the total number of unbounded Zr and Al atoms in the HY framework obtained by the ICP-MS results also support the proposed structure. This study has shown that the dealumination process can be easily performed by this electrolysis system without the use of strong acids, reactive compounds, and/or hydrothermal treatment [44]. However, the proposed model structure of $EGZrO_2$/HY depends on the amount of $EGZrO_2$ loading. Based on the FT-IR results, it was predicted that higher loading of $EGZrO_2$ gives higher probability of Si—O—Zr bond formation. This is verified by the increase in intensity of the peak at 3685 cm^{-1}, which was assigned to the hydroxyl group of extra framework aluminum species, indicating that more Al ions were dealuminated from the framework, which results in more Zr ions being replaced in the aluminosilicate framework.

3.2. Photocatalytic testing for the decolorization of MB

3.2.1. Performance of the $EGZrO_2$/HY as a photocatalyst

The performance of the prepared $EGZrO_2$/HY catalyst for the decolorization of MB was examined, and the results are shown in Fig. 7a. A controlled experiment was conducted under five different conditions including photolysis and reaction in the presence of the bare HY, $EGZrO_2$, Degussa P25 TiO_2, and $EGZrO_2$/HY catalysts. Each experiment was performed under both dark and UV-light conditions. The experiments under dark conditions removed less than 22% of the MB after 6 h of contact time, which indicated the importance of UV-light in this study. Under photolysis conditions, 9% MB was decolorized because of the degradation of the substance after

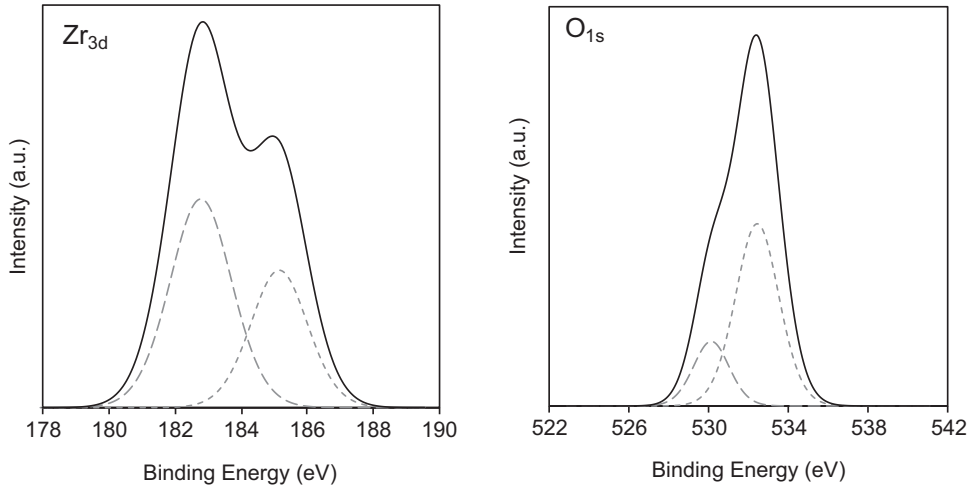

Fig. 5. XPS spectra of Zr_{3d} and O_{1s} for 22 wt% $EGZrO_2$/HY catalyst.

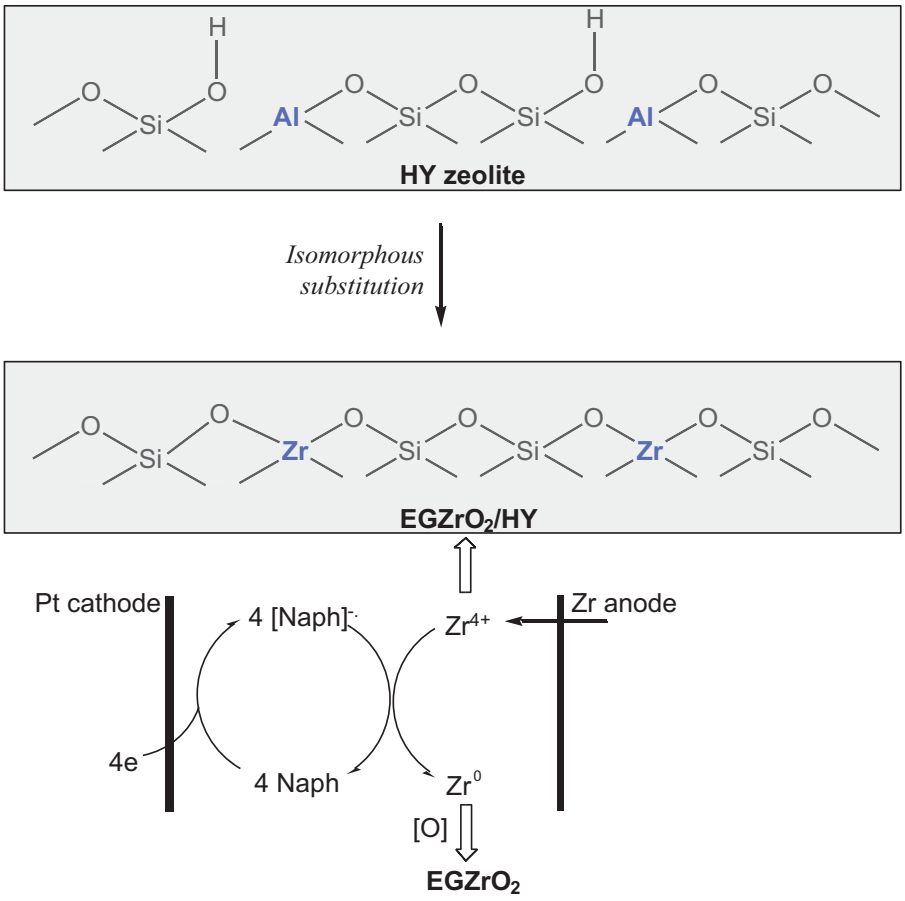

Fig. 6. Proposed mechanism for isomorphous substitution of Al with Zr in the HY zeolite structure.

long exposure to UV-light. No significant effect was observed using bare HY under dark and UV-light conditions where 22% and 30% MB was removed, respectively. The porosity of the catalyst surface may play an important role in adsorption, as previously reported in liquid–gas adsorption systems for wastewater treatment [23]. The use of $EGZrO_2$ under UV-light resulted in 40% decolorization of MB, which was eight times higher than the same reaction under dark conditions. The reaction with the TiO_2 was also carried out as a comparison and only 53% of MB was decolorized under the UV-light, indicating the lower activity of the standard metal oxide under the conditions studied. A similar result was reported in the photocatalytic decolorization of MB by immobilized TiO_2 [53]. Indeed, the removal percentage was increased up to 97% when using 1 wt% $EGZrO_2$/HY. Good distribution of the $EGZrO_2$ nanoparticles on the surface of the HY might facilitate their surface contact with UV-light and lead to higher efficiency of the reaction. This result reveals that $EGZrO_2$/HY is a potential photocatalyst semiconductor. Fig. 7b shows the changes in color before and after the reaction as well as the UV spectra of the progress of MB decolorization during 6 h of contact time.

Fig. 8a shows the UV–vis reflectance spectra of the prepared catalysts with different zirconia loading. All the $EGZrO_2$/HY catalysts show characteristic peaks of $EGZrO_2$ at a wavelength of 245 nm except the 1 wt% $EGZrO_2$/HY catalyst, which has a spectrum similar to HY. This is probably because of low $EGZrO_2$ loading and highly dominant fingerprint of HY frequencies [41]. A decrease in the $EGZrO_2$ loading resulted in a blue shift at 243 nm (22 wt% $EGZrO_2$), 240 nm (15 wt% $EGZrO_2$), and 235 nm (8 wt% $EGZrO_2$) verifying the photoreactivity of these catalysts in the UV region. In addition, the band gap energy of $EGZrO_2$ and $EGZrO_2$/HY were also determined using the Kubelka–Munk (K–M) spectrum by plotting $f_{K-M} = (hc/\lambda)^2$ as a function of $h\nu$ (Fig. 8b) [54] and compared to the band gap calculated from $E_b = 1240/\lambda$ [29]. As shown in Table 4, both the $EGZrO_2$ band gap values were similar (approximately 5.0 eV) and in agreement with the literature values [55]. An increase in $EGZrO_2$ loading resulted in a reduction in the band gap value. These results also support the suitability of this photodecolorization system for use under UV-light irradiation.

3.2.2. Effect of pH

pH is one of the most important parameters that influence the rate of photocatalytic process [56]. However, the interpretation of the effect of pH is difficult because of its multiple roles, including electrostatic interactions between the catalyst surface, solvent molecules and substrate, and charged radicals formed during the reaction [14]. Herein, the effect of pH was studied over the range of 1–11 in the presence of 1 wt% $EGZrO_2$/HY catalyst, and the results are presented in Fig. 9. Each experiment was carried out under dark conditions for 2 h to reach an adsorption–desorption equilibrium

Table 4
Calculated band gap value for each catalyst.

Catalysts	Band gap[a] (eV)	Band gap[b] (eV)
$EGZrO_2$	5.18	5.06
8 wt% $EGZrO_2$/HY	5.89	5.28
15 wt% $EGZrO_2$/HY	5.76	5.17
22 wt% $EGZrO_2$/HY	5.71	5.10

[a] Derived from plotted graph K–M versus $h\nu$ [50].
[b] Derived from Eq. $E_b = 1240/\lambda$ [29].

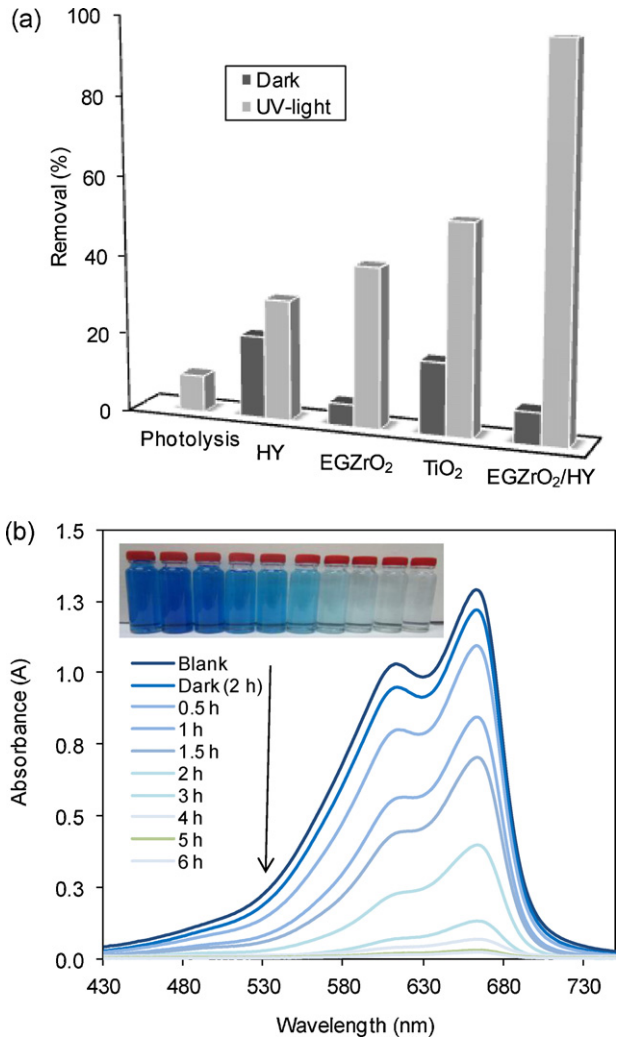

Fig. 7. (a) Photolysis and photocatalysts performance on decolorization of MB (b) color change before and after the reaction and UV spectra of the decolorization progress. (C_{MB} = 10 mg L^{-1}, pH 11, W = 0.375 g L^{-1}, t = 6 h, 1 wt% $EGZrO_2$/HY.)

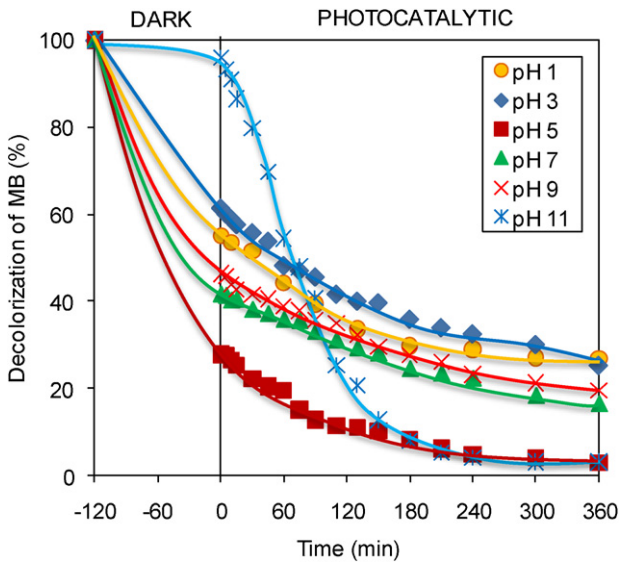

Fig. 9. Effect of pH on the decolorization of MB. (C_0 = 10 mg L^{-1}, W = 0.375 g L^{-1}, t = 6 h, 1 wt% $EGZrO_2$/HY.)

prior to photocatalytic reaction. Similar MB decolorization curves were obtained when the reactions were conducted at pH 1–9, but the reaction at pH 11 resulted in a curve with a plateau after the first 2 h under dark conditions, which then decreased rapidly when exposed to UV-light irradiation. A similar result was obtained on photodecolorization of MB by CuO/X zeolite using pH 11 as an optimum condition [26]. Under dark conditions, the highest adsorption percentage was achieved at pH 5 followed by pH 7, 9, 1, 3, and 11 because the electrostatic interaction between the negatively charged silica on the HY framework and the positively charged MB are not significantly affected by the pH environment. Thus, 72%, 58%, and 54% adsorption were observed at pH 5, 7, and 9, respectively. At lower pH values, the competition between the excess H^+ ions and MB cations on the surface of the catalyst reduced the adsorption percentage resulting in 45% and 38% MB removed at pH 1 and 3, respectively. In addition, the abundance of hydroxyl anions in the solution at pH 11 probably inhibited the MB cations

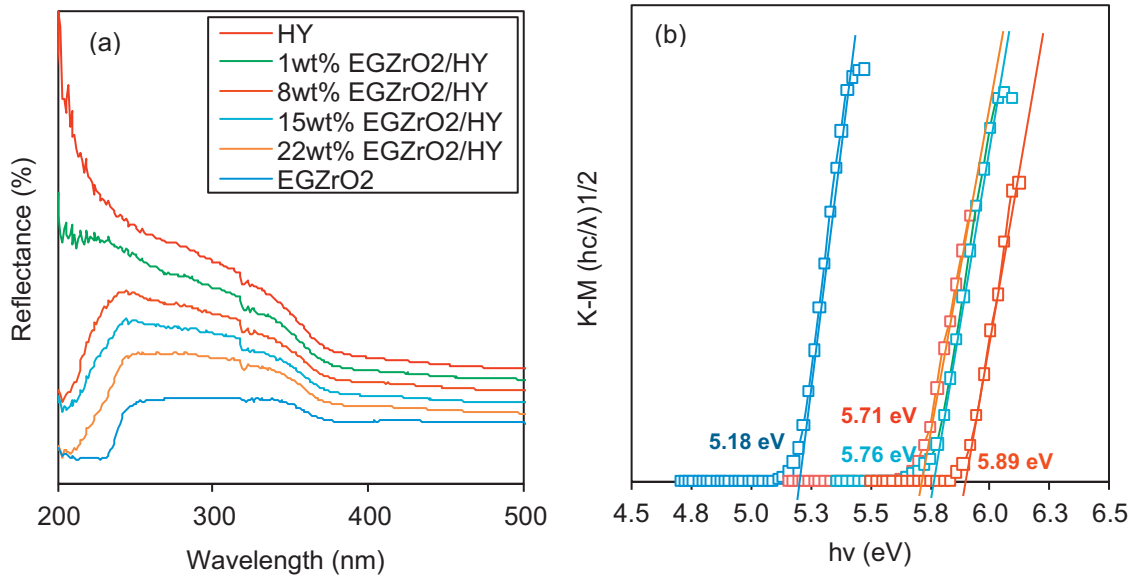

Fig. 8. (a) UV–vis reflectance and (b) the (f_{K-M}) vs. ($h\nu$) spectra of catalysts.

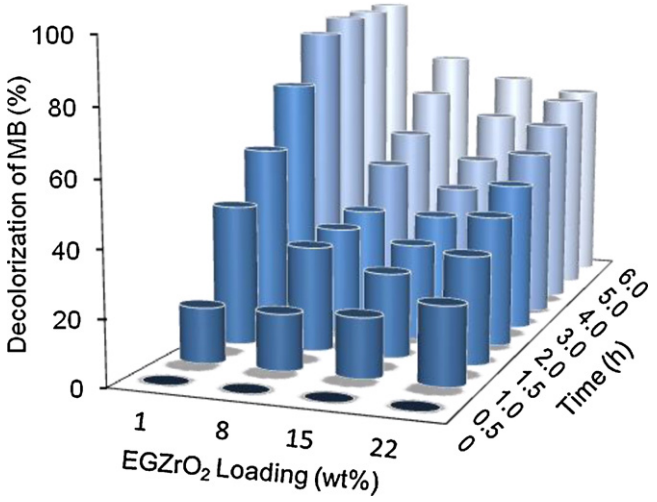

Fig. 10. Effect of $EGZrO_2$ loading on the decolorization of MB. (C_0 = 10 mg L^{-1}, pH 11, W = 0.375 g L^{-1}, t = 6 h.)

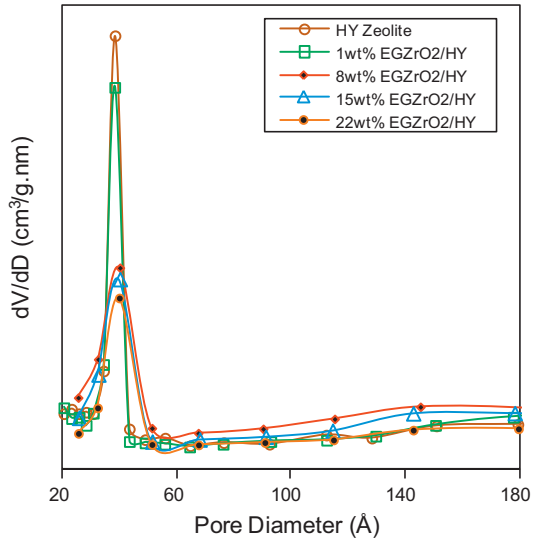

Fig. 11. Pore size distribution curves of the photocatalysts.

from being attracted directly to the catalyst surface and resulted in a lower adsorption. However, exposure of this state to UV-light facilitated and increased the formation of hydroxyl radicals leading to an increase in the photocatalytic reaction rate after the first 2 h [26] and an increase in MB decolorization up to 97% after 6 h of contact time. Less than 37% MB was decolorized at pH 1–9. The increase in the adsorption percentage resulted in a decrease of the photocatalytic ability of the catalyst due to saturation of the catalyst surface by the MB inhibiting UV-light penetration to the $EGZrO_2$.

3.2.3. *Effect of $EGZrO_2$ loading*

Fig. 10 shows the effect of $EGZrO_2$ loading (1–22 wt%) on HY. An increase in $EGZrO_2$ loading resulted in a decrease in the decolorization rate of MB, and 1 wt% of $EGZrO_2$ was found to be the optimum zirconia loading in the range studied, with the maximum decolorization of 97%, which was observed after 6 h of contact time. The surface area analysis data obtained from the BET method as well as the pore volume and pore diameter determined by the BJH desorption isotherms method can be used to verify this result. In order to provide further evidence, micropore area, micropore volume, and external surface area were estimated from *t*-plots (Table 5). The increase in $EGZrO_2$ loading decreases the surface area, micropore area, micropore volume, external surface area, and pore volume but increases the pore diameter. The decrease in the pore volume may be a reflection of the uneven particle sizes of the catalyst. A higher pore volume with a smaller pore diameter appears to enhance the photocatalytic activity [37].

In fact, the zeolite framework acts as an electron donor, which facilitates the formation of radicals for subsequent photodecolorization of MB [57]. Therefore, the increase in metal oxide loading leads to agglomeration on the support surface resulting in blockage of the pores and reduces the surface contact of HY with UV-light as well as the attraction of MB towards the catalysts surface. The pore blockage is shown by the decrease in pore volume of the catalysts (Fig. 11). In addition, as verified by the characterization data, the increase in $EGZrO_2$ loading increased the formation of Si—O—Zr bonds in the aluminosilicate framework (via isomorphous substitution). In parallel, it decreased the formation of active species $EGZrO_2$ resulting in lower photodecolorization of MB. Similar results were also reported on photoreduction of methyl orange by TiO_2 supported on a zeolite matrix [36,58]. The high crystallinity exhibited by the 1 wt% $EGZrO_2$/HY (Fig. 1a) may also explain its higher photocatalytic activity compared with the other catalysts tested [14,37].

3.2.4. *Effect of catalyst dosage*

Fig. 12 demonstrates the effect of catalyst dosage on the decolorization of MB. An increase in decolorization was observed when the catalyst dosage was increased from 0.12 to 0.375 g L^{-1}. The increase in decolorization is most likely due to an increase in the number of active sites with higher catalyst loading contributing to an increase in the number of photons and dye molecules absorbed [37]. The most effective decolorization of MB was achieved with a catalyst dosage of 0.375 g L^{-1}, and a further increase in catalyst dosage resulted in a decrease in decolorization. A higher particle concentration leads to a higher turbidity of the suspension, which reduces light penetration and inhibits photodecolorization [58].

3.3. *Kinetic analysis*

To study the kinetics of MB photodecolorization, a series of reactions at different initial concentrations of MB ranging from 10 to 100 mg L^{-1} at pH 11 were performed. In general, the influence of the initial concentration of the solution on the photocatalytic decolorization rate of most organic compounds is described by pseudo first-order kinetics, which is rationalized in terms of the

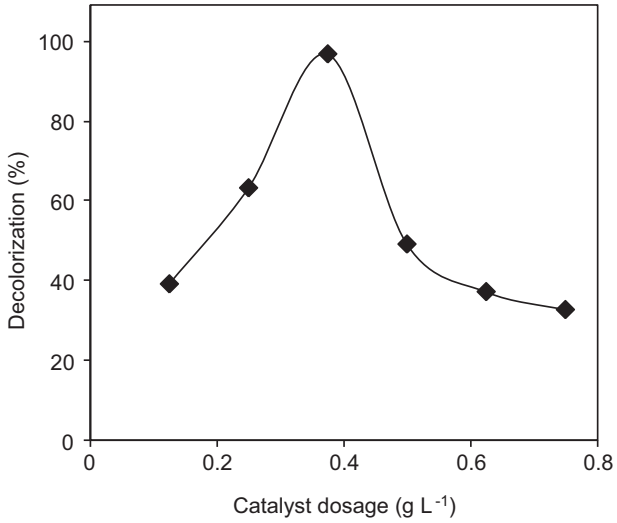

Fig. 12. Effect of catalyst dosage on the decolorization of MB. (C_0 = 10 mg L^{-1}, pH 11, t = 6 h, 1 wt% $EGZrO_2$/HY.)

Table 5
The textural properties of the catalysts.

Catalysts	Surface area ($m^2\ g^{-1}$)	External surface area ($m^2\ g^{-1}$)	Micropore area ($m^2\ g^{-1}$)	Average pore diameter[a] (nm)	Micropore volume ($cm^3\ g^{-1}$)	Pore volume ($cm^3\ g^{-1}$)
$EGZrO_2$	54.9	51.7	3.16	11.1	0.0013	0.153
HY	654	195	459	2.73	0.2126	0.447
1 wt% $EGZrO_2$/HY	649	193	456	2.75	0.2069	0.445
8 wt% $EGZrO_2$/HY	551	175	376	3.32	0.1667	0.426
15 wt% $EGZrO_2$/HY	493	169	324	3.41	0.1590	0.408
22 wt% $EGZrO_2$/HY	447	167	280	3.45	0.1468	0.382

[a] Adsorption average pore diameter (4, v/v by BET).

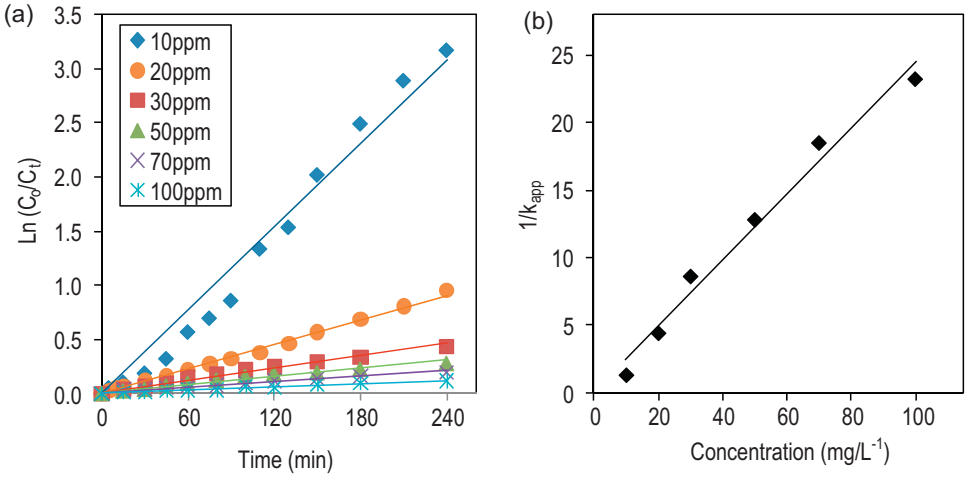

Fig. 13. (a) Photodecolorization kinetics of MB using 1 wt% $EGZrO_2$/HY at different MB concentrations and (b) the relationship between $1/k_{app}$ and the initial concentration of MB.

Langmuir–Hinshelwood model modified to accommodate reactions occurring at solid–liquid interface [59]. At low initial dye concentrations, the simplest equation for the rates of photodecolorization of MB is given by [60],

$$\ln C_t = -kt + \ln C_0 \tag{5}$$

where k is the pseudo first-order rate and C_0 and C_t are the concentrations of MB at initial time and time t, respectively. The integration of Eq. (5) yields Eq. (6),

$$\ln\left(\frac{C_0}{C_t}\right) = kt \tag{6}$$

The straight line resulting from a plot of $\ln(C_0/C_t)$ as a function of time shown in Fig. 13a confirmed that MB photodecolorization catalyzed by $EGZrO_2$/HY follows first-order kinetics. The slope of the line is the apparent first-order rate constant (k_{app}). The values of k obtained from our experiments are listed in Table 6 and reveal a significant and favorable effect of $EGZrO_2$/HY on the photodecolorization of MB. A lower concentration of MB results in a higher first-order rate constant, demonstrating the suitability of the system for low dye concentrations. Indeed, the concentrations of dyes in the wastewater from textile industry effluents are always low [61].

Table 6
The parameters of photodecolorization at different initial concentrations of MB.

Initial concentration ($mg\ L^{-1}$)	Reaction rate, k (h^{-1})	Initial reaction rate, r_0 ($mg\ L^{-1}\ h^{-1}$)	Decolorization (%)
10	0.771	7.71	96.7
20	0.227	4.54	75.3
30	0.116	3.48	43.0
50	0.078	3.90	31.8
70	0.054	3.78	22.2
100	0.043	4.30	12.2

Hypothetically, the photodecolorization of MB by $EGZrO_2$/HY could be an interface process [60] that might follow the Langmuir–Hinshelwood model (Eqs. (7) and (8)),

$$r_0 = -\frac{dC}{dt} = \frac{K_R K_{LH} C_0}{1 + K_{LH} C_0} = k_{app} C_0 \tag{7}$$

$$\frac{1}{k_{app}} = \frac{1}{K_R K_{LH}} + \frac{C_0}{K_R} \tag{8}$$

where K_R is the reaction rate constant and K_{LH} is the Langmuir–Hinshelwood adsorption equilibrium constant.

A linear plot was obtained by plotting $1/k_{app}$ as a function of C_0 (Fig. 13b), indicating that the photodecolorization of MB by $EGZrO_2$/HY is consistent with the Langmuir–Hinshelwood model. The reaction rate constant and the adsorption equilibrium constant were calculated to be $K_R = 4.08\ mg\ L^{-1}\ h^{-1}$ and $K_{LH} = 6.45\ L\ mg^{-1}$, respectively. Because the value of K_{LH} is larger than K_R, these results suggested that the reaction would occur in the bulk solution as well as at the surface of the catalyst [62]. In addition, the number of adsorption sites may not be abundant enough to initiate the reaction [63].

3.4. Leaching and reusability studies

To study the effect of zirconia leaching into the solution, the samples were kept in the dark for 2 h and then irradiated under UV light for 2, 4, and 6 h before being subjected to ICP-MS. The result shows that no Zr ions were detected, indicating that the photocatalytic occurrence is mainly due to Zr that exists on the catalyst surface.

A repeated experiment was carried out using 1 wt% $EGZrO_2$/HY catalyst in order to study the stability of the catalyst for MB

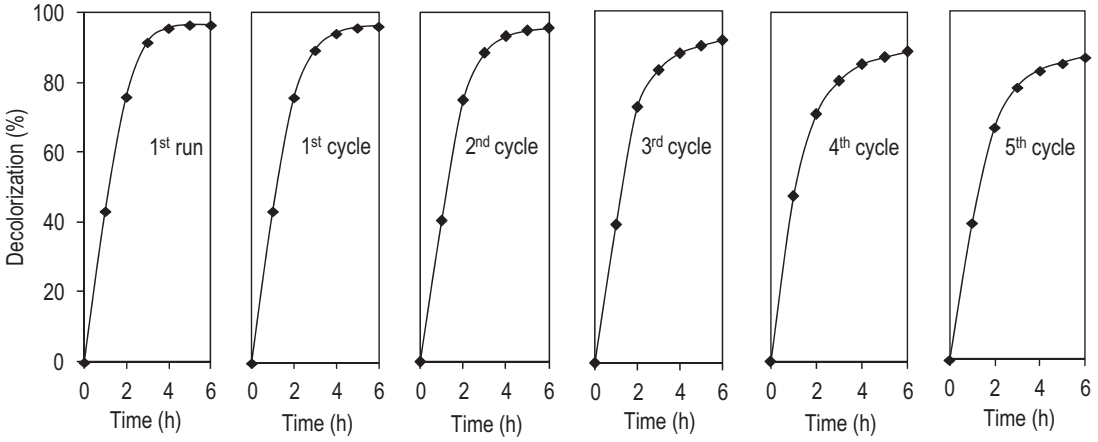

Fig. 14. Reusability of 1 wt% $EGZrO_2$/HY on the photocatalytic decolorization of MB. (C_0 = 10 mg L^{-1}; pH 11; W = 0.375 g L^{-1}; t = 6 h.)

decolorization (Fig. 14). The initial concentration of MB was kept constant (10 mg L^{-1}) at pH 11 and 6 h of irradiation time, and the catalyst was recycled after filtration and calcination at 823 K for 3 h at every cycle. It can be observed that after five repeated experiments, the catalyst was still active with just small decreases from 96.7% to 86.9% of decolorization percentage. The heat treatment most probably induced the catalyst aggregation after several recycles, which resulted in the decrease of surface area and finally led to the decrease of photocatalytic efficiency [64].

3.5. Investigation on biodegradability

In the present case, COD is indirectly determined to investigate the amount of organic compounds present in the aqueous solution (Fig. 15). The initial COD value of dye solution of concentration 10 mg L^{-1} was measured as 144 mg L^{-1}. The percentage of COD removal increased drastically in the first 1 h of reaction and slowed up to 2 h, then the rate increased drastically again before achieving equilibrium after 6 h of reaction. The former fast reaction may be because of the degradation of the MB into two different compounds known as hydroxylated and amine substituent products. Next, the hydroxylated compound was converted into a sulfoxide form under a slow reaction. The latter mineralization of amine substituent and spontaneous oxidation followed by ring opening of phenolic compounds contributed in the formation of CO_2 and H_2O under fast reaction [2,26]. For TOC reduction, it shows a significant decrease in terms of the TOC/TOC_0 ratio. This sort of decrease may attribute to the fact that structured dye molecules were fragmented and converted into small organic molecules, which subsequently enhances the mineralization during the irradiation process [65]. In addition, the five days (BOD_5) was evaluated to measure the amount of oxygen consumed by a microorganism to degrade organic matter during a five days period. Note that the BOD_5/COD ratio can be used as a biodegradability index for the aqueous dye solution. Therefore, the BOD_5/COD ratio of the non-irradiated dye solution was observed to be 0.26, which indicates that the dye solution is non-biodegradable. After 6 h of irradiation, the BOD_5/COD ratio was increased up to 7.14 because of the formation of more biodegradable intermediates during the photodegradation. The higher value of BOD_5/COD ratio will give better biodegradability, as reported in literature [66]. In order to provide some evidence, the changes of the pH solution before and after reaction were monitored, showing that the solution pH 11 was shifted to pH 7.8, respectively. It was reflected that the MB dye was oxidized and decomposed to some extent as CO_2 and H_2O [67].

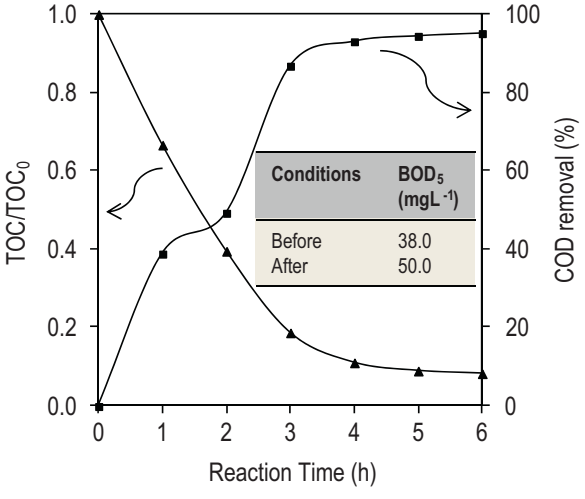

Fig. 15. The graph of COD removal and TOC reduction levels after 6 h of reaction and the insert table are its corresponding BOD_5.

4. Conclusions

In this study, an $EGZrO_2$/HY catalyst was prepared by a simple electrochemical method. The physicochemical properties of the prepared catalysts were studied by XRD, TEM, FT-IR, UV–vis/DRS, surface area analysis, ^{29}Si and ^{27}Al MAS NMR, XPS, and ICP-MS. The dealumination of the Al from the HY framework accompanied by an ion exchange with Zr^{4+} appears to be the primary reason for the observed effectiveness of the $EGZrO_2$/HY catalyst compared to bare $EGZrO_2$ and HY. However, the presence of more Si—O—Zr bonds in the framework through isomorphous substitution inhibits the photodecolorization activity. 0.375 g L^{-1} 1 wt% $EGZrO_2$/HY was found to provide the optimum loading, which resulted in 97% decolorization at pH 11 after 6 h of contact time when the catalysts were evaluated for the decolorization of MB under UV-light irradiation. The kinetic studies showed that the decolorization followed pseudo first-order kinetics, and the rate constants determined using the Langmuir–Hinshelwood model are K_R = 4.08 mg $L^{-1}h^{-1}$ and K_{LH} = 6.45 L mg^{-1}. Active catalytic ion species (Zr^{4+}) may play an important role in the formation of hydroxyl ($HO^{\bullet}$), hydrogen peroxides ($HO_2^{\bullet}$), and superoxide ($^{\bullet}O_2^-$) radicals used in the decolorization reaction. In addition, measurements of the mineralization of MB by COD removal, BOD_5/COD, and TOC/TOC_0 ratio analysis give 95%, 7.14, and 0.08, respectively, after 6 h of contact time. The structure and morphology of the catalyst were still stable after five cycles and the leaching test showed negligible leaching effect. Because of

the simple process of preparing the catalyst and the low amount of metal loading required, this system exhibits great potential for improving the quality of wastewater discharged from the textile industry and other industries.

Acknowledgements

The authors are grateful for the financial support by the Research University Grant from Universiti Teknologi Malaysia (Grant No. 01H59), the awards of UTM Zamalah Scholarship (Norzahir Sapawe), and to the Hitachi Scholarship Foundation for their support.

References

[1] S. Ameen, M.S. Akhtar, Y.S. Kim, H.S. Shin, Applied Catalysis B: Environmental 103 (2011) 136–142.
[2] A. Houas, H. Lachheb, M. Ksibi, E. Elaloui, C. Guillard, J.M. Herrmann, Applied Catalysis B: Environmental 31 (2001) 145–157.
[3] F.M. Darus, H.J. Hashim, R. Laiman, M.N. Yusoff, Proc. Prosiding Seminar Kebangsaan Pengurusan Persekitaran, UKM Malaysia, 2005, pp. 301–308.
[4] B.H. Hameed, E. Khaiary, Journal of Hazardous Materials 155 (2008) 601–609.
[5] K. Kadirvelu, M. Kavipriya, C. Karthika, M. Radhika, N. Vennilamani, S. Pattabhi, Bioresource Technology 87 (2003) 129–132.
[6] O. Hamdaoui, M. Chiha, Acta Chimica Slovenica 54 (2007) 407–418.
[7] C.S.D. Rodrigues, L.M. Madeira, R.A.R. Boaventura, Journal of Hazardous Materials 172 (2009) 1551–1559.
[8] A.A. Jalil, S. Triwahyono, S.H. Adam, N.D. Rahim, M.A.A. Aziz, N.H.H. Hairom, N.A.M. Razali, M.A.Z. Abidin, M.K.A. Mohamadiah, Journal of Hazardous Materials 181 (2010) 755–762.
[9] F. Harrelkas, A. Azizi, A. Yaacoubi, A. Benhammou, M.N. Pons, Desalination 235 (2009) 330–339.
[10] M. Panizza, G. Cerisola, Applied Catalysis B: Environmental 75 (2007) 95–101.
[11] J.S. Wu, L.H. Liu, K.H. Chu, S.Y. Suen, Journal of Membrane Science 309 (2008) 239–245.
[12] R.A. Damodar, S.J. You, S.H. Ou, Separation and Purification Technology 78 (2010) 64–71.
[13] D. Robert, Catalysis Today 122 (2007) 20–26.
[14] N. Talebian, M.R. Nilforoushan, Thin Solid Films 518 (2010) 2210–2215.
[15] M. Aleksic, H. Kusic, N. Koprivanac, D. Leszczynska, A.L. Bozic, Desalination 257 (2010) 22–29.
[16] W. Zhou, K. Liu, H. Fu, K. Pan, L. Zhang, L. Wang, C.C. Sun, Nanotechnology 19 (2008) 1–7.
[17] M.J. Height, S.E. Pratsinis, O. Mekasuwandumrong, P. Praserthdam, Applied Catalysis B: Environmental 63 (2006) 305–312.
[18] X. Yang, C. Cao, L. Erickson, K. Hohn, R. Maghirang, L. Klabunde, Applied Catalysis B: Environmental 91 (2009) 657–662.
[19] A. Franco, M.C. Neves, M.M.L. Mobteiro, Journal of Hazardous Materials 161 (2009) 545–550.
[20] J.H. Sun, S.Y. Dong, J.L. Feng, X.J. Yin, X.C. Zhao, Journal of Molecular Catalysis A: Chemical 335 (2011) 145–150.
[21] W. Zhao, L. Feng, R. Yang, J. Zheng, X. Li, Applied Catalysis B: Environmental 103 (2011) 181–189.
[22] W. Zhang, K. Wang, Y. Yu, H. He, Chemical Engineering Journal 163 (2010) 62–67.
[23] H. Chen, A. Matsumoto, N. Nishimiya, K. Tsutsumi, Colloids and Surfaces A 57 (1999) 295–305.
[24] X. Liu, K.K. Iu, J.K. Thomas, Journal of the Chemical Society, Faraday Transactions 89 (1993) 1861–1865.
[25] Z.M. El-Bahy, M.M. Mohamed, F.I. Zidan, M.S. Thabet, Journal of Hazardous Materials 153 (2008) 364–371.
[26] A. Nezamzadeh-Ejhieh, S. Hushmandrad, Applied Catalysis A-General 388 (2010) 149–159.
[27] R. Prihodko, I. Stolyarova, G. Gunduz, O. Taran, S. Yashnik, V. Parmon, V. Guncharuk, Applied Catalysis B: Environmental 104 (2011) 201–210.
[28] N. Chandra, D.K. Singh, M. Sharma, R.K. Upadhyay, S.S. Amritphale, S.K. Sanghi, Journal of Colloid and Interface Science 342 (2010) 327–332.
[29] L.Y. Zhu, X.Q. Wang, G.H. Zhang, Q. Ren, D. Xu, Applied Catalysis B: Environmental 103 (2011) 428–435.
[30] B. Neppolian, Q. Wang, H. Yamashita, H. Choi, Applied Catalysis A-General 333 (2007) 264–271.
[31] G. Tian, K. Pan, H. Fu, L. Jing, W. Zhou, Journal of Hazardous Materials 166 (2009) 939–944.
[32] A.A. Jalil, N. Kurono, M. Tokuda, Synlett 12 (2001) 1944–1946.
[33] S. Triwahyono, A.A. Jalil, M. Musthofa, Applied Catalysis A-General 372 (2010) 90–93.
[34] N.F. Jaafar, A.A. Jalil, S. Triwahyono, M.N.M. Muhid, N. Sapawe, M.A.H. Satar, H. Asaari, Chemical Engineering Journal 191 (2012) 112–122.
[35] Q. Chang, J.E. Zhou, Y. Wang, G. Meng, Advanced Powder Technology 20 (2009) 371–374.
[36] J. Yang, J. Zhang, L. Zhu, S. Chen, Y. Zhang, Y. Tang, Y. Zhu, Y. Li, Journal of Hazardous Materials B137 (2006) 952–958.
[37] D.P. Das, N. Baliarsingh, K.M. Parida, Journal of Molecular Catalysis A: Chemical 261 (2007) 254–261.
[38] C.J. Lucio-Ortiz, J.R. De la Rosa, A. Hernandez-Ramirez, E.M. Lopez-Cuellar, G. Beltran-Perez, R.D.C.M. Guardiola, Colloids and Surfaces A: Physicochemical and Engineering Aspects 371 (2010) 81–90.
[39] A. Mondal, S. Ram, Ceramics International 30 (2004) 239–249.
[40] C. Wang, H. Shi, Y. Li, Applied Surface Science 257 (2011) 6873–6877.
[41] S. Kongwudthiti, P. Praserthdam, W. Tanakulrungsank, M. Inoue, Journal of Materials Processing Technology 136 (2003) 186–189.
[42] M. Noorjahan, V.D. Kumari, M. Subrahmanyam, L. Panda, Applied Catalysis B: Environmental 57 (2005) 291–298.
[43] H.D. Lutz, J. Henning, H. Haeuseler, Journal of Molecular Structure 156 (1987) 143–145.
[44] S. Krijnen, Titanium Epoxidation Catalysts: Zeolite and Silsesquioxane based Materials, Eindhoven University of Technology, Netherlands, 1998.
[45] J. Klinowski, Progress in Nuclear Magnetic Resonance Spectroscopy 16 (1984) 237–309.
[46] J. Klinowski, Colloids and Surfaces A 36 (1989) 133–154.
[47] Z. Luan, C.F. Cheng, H. He, J. Klinowski, Journal of Physical Chemistry 99 (1995) 10590–10593.
[48] B. Wu, R. Yuan, X. Fu, Journal of Solid State Chemistry 182 (2009) 560–565.
[49] L. Armelao, C.E. Sittner, M. Groenewolt, S. Gross, C. Sada, U. Schubert, E. Tondelloa, A. Zattina, Journal of Materials Chemistry 15 (2005) 1838–1848.
[50] D. Barreca, M.P. Copley, A.E. Graham, J.D. Holmes, M.A. Morris, R. Seraglia, T.R. Spalding, E. Tondello, Applied Catalysis A-General 304 (2006) 14–20.
[51] Y. Ohtsu, M. Egami, H. Fujita, K. Yukimura, Surface and Coatings Technology 196 (2005) 81–84.
[52] J.Z. Kong, A.D. Li, X.Y. Li, H.F. Zhai, W.Q. Zhang, Y.P. Gong, H. Li, D. Wu, Journal of Solid State Chemistry 183 (2010) 1359–1364.
[53] W.S. Kuo, P.H. Ho, Chemosphere 45 (2001) 77–83.
[54] H. Jia, H. Xu, Y. Hu, Y. Tang, L. Zhang, Electrochemistry Communications 9 (2007) 354–360.
[55] J. Portier, H.S. Hilal, I. Saadeddin, S.J. Hwang, M.A. Subramanian, G. Campet, Progress in Solid State Chemistry 32 (2004) 207–217.
[56] H. Lachheb, E. Puzenat, A. Houas, M. Ksibi, E. Elaloui, C. Guillard, J.M. Herrmann, Applied Catalysis B: Environmental 39 (2002) 75–90.
[57] R. Chatti, S.S. Rayalu, N. Dubey, N. Labhsetwar, S. Devotta, Solar Energy Materials and Solar Cells 91 (2007) 180–190.
[58] E. Bizani, K. Fytianos, I. Poulios, V. Tsiridis, Journal of Hazardous Materials 1367 (2006) 85–94.
[59] C.S. Turchi, D.F. Ollis, Journal of Catalysis 122 (1990) 178–192.
[60] L.Y. Yang, S.Y. Dong, J.H. Sun, J.L. Feng, Q.H. Wu, S.P. Sun, Journal of Hazardous Materials 179 (2010) 438–443.
[61] J. Grzechulska, A.W. Morawski, Applied Catalysis B: Environmental 36 (2002) 45–51.
[62] J. Cunningham, G. Al-Sayyed, Journal of the Chemical Society, Faraday Transactions 86 (1990) 3935–3941.
[63] Y. Meng, X. Huang, Y. Wu, X. Wang, Y. Qian, Environmental Pollution 117 (2002) 307–313.
[64] M. Huang, C. Xu, Z. Wu, Y. Huang, J. Lin, J. Wu, Dyes and Pigments 77 (2008) 327–334.
[65] J. Paul, K.P. Rawat, K.S.S. Sarma, S. Sabharwal, Applied Radiation and Isotopes 69 (2011) 982–987.
[66] K. Swaminathan, K. Pachhade, S. Sandhya, Desalination 186 (2005) 155–164.
[67] X. Li, K. Lv, K. Deng, J. Tang, R. Su, J. Sun, L. Chen, Materials Science and Engineering B 158 (2009) 40–47.